SVU-International Journal of Engineering Sciences and Applications (2024) 5(2): 265-274
Print ISSN 2785-9967 | Online ISSN 2735-4571
DOI 10.21608/SVUSRC.2024.288391.1218

Study of Tube Ends Forming Using Ballizing Technique

Muhammad M. Abo Hussain [1,□], M. N. Elsheikh [2], Yehia M. Ismaael [3], S. Z. El-Abden [3] and Essam K. Saied [4]

Abstract The fabrication of tube ends is an important branch in the fluid and gas transportation industries as it is needed in pipes connection process. Traditional methods like pressing, stamping, and welding with flanges have been utilized, along with non-traditional techniques such as spinning and rotary forging. Steel balls were exploited in this study as a forming tool for aluminum pipe ends. To select the proper machine and found the necessary forces for forming, a mathematical approach was created to estimate the forming load. The forming tool was made up of two steel balls with a diameter of 45 mm that could move freely around their three axes. The combination of the steel balls above the thrust bearing in its holder is mounted on a jaws of lathe chuck which acting as a holder for the whole tool. The forming process began by adjusting the contact of the forming ball with the outer surface of the pipe, moving the carriage backward, and adjusting the forming depth. As the forming ball contacted the pipe's outer surface and advanced until the desired nosing ratio was achieved, the forming occurred. The effects of these variables on the forming forces, hardness, and thickness change of the formed part were evaluated. The experimental results showed enhancement in reduction ratios to reach 63% compared to a ratio of about 40%. The thickness change values after forming were within acceptable limits of 12%. The results of the mathematical model aligned with the experimental findings.

Keywords: Metal spinning; Tube end, Nosing; Theoretical approach; Nosing load and nosing ratio.

1 Introduction

The spinning process can be used to produce a variety of shapes, such as conical, spherical, and cylindrical. The spinning process is more efficient than the traditional methods, as it produces a better finish and requires less time. The spinning process also has the advantage of being able to produce complex shapes with greater accuracy [1]. Pipes are used in many applications to carry fluid from one place to another. Pipes are manufactured with standard lengths and there are several ways to join pipes. The type of joining depends on the material of the pipe and the purpose for which it is used. For instant welding, flanges, sockets, clamped joints, union joints, and nosing with flaring joints are the most common types of joining pipes. The tube nosing is manufactured by traditional methods, such as a punch and die. The tube nosing can also be produced by spinning processes [2].

Yasser O. Ibrahim et al. evaluated the performance of a novel spinning multifunction tool through an experimental study. The tool was employed for a nosing process, and the results demonstrated a positive correlation between the maximum load and the nosing ratio (NR = D/d). This correlation showed an increase of up to 41% in maximum loads with increasing nosing ratios. [3]. Ahmed Hamzawi et al. presented a new spinning multifunction tool and used it for flaring. The results were investigated using a compound tool, and a parametric study was carried out to explain the influence of these working conditions on the thickness variation, nosing loads, and surface hardness [4]. Wataru Obaa et al. presented A two-step rotary nosing process with relieved dies was investigated to reduce tube tip defects. The relieved surfaces weaken the axial pushing force, mitigating buckling, and reduce compressive hoop stress, preventing wrinkles. This approach led to a 9% improvement in the forming limit compared to a single-step process under optimal conditions. [5]. Tong Wen et al. This study investigated a novel single-point incremental forming method for crimping open tube ends. The results demonstrate the method's potential for small-batch production of tubes with customized end geometries. [6]. Steve Wilsona et al. investigated a novel spinning process for producing offset tubes. The process utilizes a standard boring head mounted in a lathe chuck to hold the tube and a roller for forming. This approach

Received: 9 May 2024/ Accepted: 17 July 2024
□Corresponding Author : Muhammad M. Abo Hussain, E-mail Muhammad.mustafa24666@gmail.com
1. Department of Production Engineering and Mechanical Design, Faculty of Engineering, Minia University, Egypt.
2. Department of Mechanical Engineering, Faculty of Technology and Education, Beni-Suef University, Beni-Suef 62511, Egypt.
3. Department of Production Engineering and Mechanical Design, Faculty of Engineering, Minia 61111, Egypt
4. Department of Mechanical Engineering, Faculty of Engineering, Beni-Suef University, Beni-Suef 62511, Egypt

demonstrates the feasibility of creating offset tubes at a lower cost, eliminating the need for specialized spinning equipment. [7]. Chi-Chen Huang et al. investigated the neck spinning process for elevated-temperature tube ends using a roller tool on six-step spun tubes. An optimization technique identified the ideal forming path, which was subsequently validated through experiments. [8]. Yao Jianguo and Murata Makoto investigated the effects of tube end spinning using a roller pair. The results showed that thinner tubes with larger spinning pitches exhibited increases in thickness strain, spinning force, twist angle, and surface roughness. Conversely, thinner tubes with smaller spinning pitches experienced higher axial strain and improved diametric accuracy. [9].

Yao Jianguo and Murata Makoto carried out the effect of processing branch on tube end spinning using roller tools. Tubes were spun with two progressive geometries: a taper region (branch A) and a taper angle (branch B). Results showed that branch A (taper region) produced lower spinning force, elongation strain, and wall thickness compared to branch B (taper angle). [10].

Chi-Chen Huang et al. introduced a numerical simulation to investigate the neck-spinning process of tubes at high temperatures, employing two rollers. The results achieved excellent agreement with experimental data. Notably, the simulations revealed a significant increase in the twisting angle between the top and bottom of the spun tube as the coefficient of friction increased. [11]. Takashi Kuboki et al. presented a novel rotary reduction method for tube tips, employing a specially designed die with relief surfaces. The effectiveness of the method is validated through a combination of experimental trials and numerical analysis. [12].

Fouly A. Mohamed et al. developed a novel approach for flanging deformed tube ends using a ball-shaped tool. Our investigation confirmed the process's success in achieving the desired flange shape. [13]. Yong Li et al. utilizes finite element analysis (FEA) to investigate the tube sinking process of a thin-walled copper tube. The analysis compares the effects of two and three-split dies on the strain distribution during a radial forging process without a mandrel. The results demonstrate that the three-split die configuration promotes a more uniform strain distribution within the thin-walled tube compared to the two-split die configuration under identical process conditions. [14]. Yoichi Takahashi et al., combined experimental and three-dimensional finite element simulations to explore how tube neck length influences cracking during the tube spinning process. Two rollers with a 100 mm outer diameter and an 8.0 mm curvature radius were used to simulate spinning. The results revealed a significant decrease in the tube thickness ratio within the tapered section, followed by a thickening towards the tube end. This marked thinning at the corner of the tapered section was identified as the primary cause of cracking. [15]. Chun-jiang Zhao1 et al., presents a computational model for calculating the three-dimensional forces acting on a spinning ball. The model was developed and validated using a 7 mm diameter ball as a reference. The validation involved testing the axial component of the force, confirming the model's accuracy for predicting the overall spinning force. [16]. Zhao Chunjiang et al., presented a novel method for machining an annular groove on the inner surface of a steel tube using ball spinning.

The process was investigated with GCr15, a hot bearing steel. The results indicate a positive correlation between ball diameter, feed rate, and spinning pressure. Additionally, the tangential spinning pressure exhibits a linear relationship with the depth of spinning. [17].

M Kuss and B. Buchmayr investigated the impact of various parameters on computational time in 3D FEM simulations. A ball bearing with eight balls was used as a forming tool in the simulations. The results revealed a trend: increasing the axial feed rate could lead to a process design that minimizes damage while reducing computational time. [18].

Shuyong Jiang et al., reported a novel technique called backward ball spinning to fabricate a composite tube composed of copper and aluminum. The experimental findings closely matched the simulations, and interestingly, the outer aluminum layer exhibited greater axial elongation compared to the inner copper layer in the Cu-Al composite tube. [19].

N Akkusa et al. investigated a dome-forming of seamless aluminum tubes using a novel two-step spinning process. Experimental and analytical approaches were employed to analyze the process. The results demonstrate that the proposed method achieves a thicker boss region compared to conventional forming. Additionally, the final boss thickness is influenced by its length, with longer bosses exhibiting greater thickness. [20].

Q.X. Xia a, et al., presented a novel spinning technology for creating asymmetrical hollow parts. This technology has been investigated using a 170 mm diameter roller. Notably, the simulations yielded results that closely matched the experimental findings, demonstrating the technology's validity. [21].

Zhiyong XUE, et al. investigated neck spinning of pipes using a simulation. The simulation involved nine spinning

passes at 360 °C with a 400 mm x 100 mm x 15 mm roller. Results showed maximum deformation at the pipe mouth, and interestingly, the thickness of the neck deformation zone decreased with increasing feeding rate. [22].

Essam K. Saied, et al. suggested a novel compound tool designed to perform both conventional spinning and flow-forming processes in a single operation. The tool integrates two rollers for conventional spinning and two balls for concurrent flow-forming. Experimental validation was conducted through multiple compound processes using the tool to manufacture thin-walled cups. The results successfully verified the tool's effectiveness. [23].

Chin-Tarn Kwan employed finite element analysis to investigate the tube nosing process with an eccentric conical die. The results revealed a negative correlation between the critical nosing ratio and the material's strain hardening exponent. [24].

C.-T. Kwan studied A combined experimental and analytical investigation explored the influence of various parameters on the tube nosing process using SKD11 (JIS) die steel. These parameters included tube wall thickness, die angle, material strength coefficient, strain hardening exponent, billet length, and die fillet radius. [25].

Ken-Ichi Manabe and Hisashi Nishimura Studied An investigation into the tube nosing process with conical dies was conducted through a combined experimental and analytical approach. The results revealed that a circular die design led to a reduction in nosing load and an increase in the nosing limit. [26].

B.P.P. Gouveia, et al. A combined theoretical and experimental investigation explored the process of beading and nosing tubes with dies. The results demonstrated that lubrication significantly reduces the forming load, thereby enhancing the formability of the tubes. Furthermore, the finite element method can be employed to construct a formability diagram, which predicts the success or failure of a desired nosing ratio. [27].

Hua Yang, et al. A three-dimensional finite element model was developed to simulate three-roller backward tube spinning. The simulation predicted a significant diameter reduction of up to 40%. [28].

Makoto Murata et al. investigated the formability of magnesium tubes using a heated roller in a spinning process. The effects on the formed parts' mechanical properties, particularly hardness and diameter accuracy, were evaluated. [29].

Yao Jianguo and Murata Makoto investigated the influence of feed per pass on the nosing process using the same eccentric conical die. Employing two rollers, the analysis revealed a positive correlation between the indented feed and the resulting spinning force. [30].

Q.X. Xia et al. presented a simulation of a non-axisymmetric nosing process using MARC, a 3D elastoplastic finite element software. The simulation results exhibited excellent agreement with experimental data, achieving a deviation of less than 10%. [31].

S. Z. El-Abden and Raghad Atef investigated hub forming through hole expansion using conical, flat, and spherical punches, employing both theoretical and experimental approaches. The results aimed to establish limiting processing curves that would differentiate safe and unsafe forming regions. [32].

S. Z. El-Abden introduced a novel single-pass plastic deformation technique for joining dissimilar sheet and tube materials. The design incorporates a new punch to ensure control over the internal tube diameter. Finite element (FE) analysis results demonstrated good agreement with experimental observations regarding the deformation stages, validating the effectiveness of the proposed technique. [33].

K. M. Attia, et al., presentd a novel, single-stroke technique for performing conventional spinning, wall thickness reduction, and burnishing. A newly developed tool accomplishes these three operations simultaneously. The tool features a three-stage design: rollers for conventional spinning, followed by balls for wall thickness reduction, and finally, spring-loaded balls for burnishing. Experimental analysis identified the optimal forming load conditions at a rotational speed of 150 rpm, axial feed of 0.3 mm/rev, and burnishing load of 25 kN. [34].

Rania Ali Abdelhamid, et al., utilized theoretical analysis and the finite element method (FEM) was employed to investigate the forming of commercial aluminum tubes into conical and hemispherical dies. The results demonstrated good agreement between the analytical predictions and the FEM simulations. [35].

A review of existing literature indicates that the prevailing methods for tube nosing rely on punch and die techniques or CNC machining. While effective, these approaches can be expensive and time-consuming. This study proposes an alternative approach utilizing a novel metal spinning tool for tube nosing.

This innovative technique offers significant advantages, particularly in terms of reduced cost and processing time. This paper introduces a novel method for end nosing of

tubes using metal spinning with a ballizing technique.

The proposed tool utilizes forming balls, which are predicted to yield a superior surface finish on the workpiece. Additionally, the reduced contact area between the tool and the tube is expected to achieve a high nosing ratio and lower process loads compared to conventional methods.

Experimental validation was conducted on aluminum tubes. The Ballizing tool was designed based on the desired nosing ratio. Key process parameters, including axial feed rate (f in mm/rev), rotating speed (n in rpm), and nosing ratio (NR), were investigated using various values during the fabrication of nosed tube specimens.

A combined experimental and mathematical analysis was employed to evaluate the nosing loads and the characteristics of the formed parts.

2 Analytical Model of Nosing Loads.

Fig. 1 depicts the process of forming the end of the pipes, with two distinct halves: the left half displays the process before forming, while the right half shows the model of the pipe that is to be created.

A theoretical analysis of the nosing load was conducted to select a suitable machine for the process. The aim of the analysis is to estimate the forming loads, torque, and power needed to complete the process in order to choose the suitable machine and its capacity.

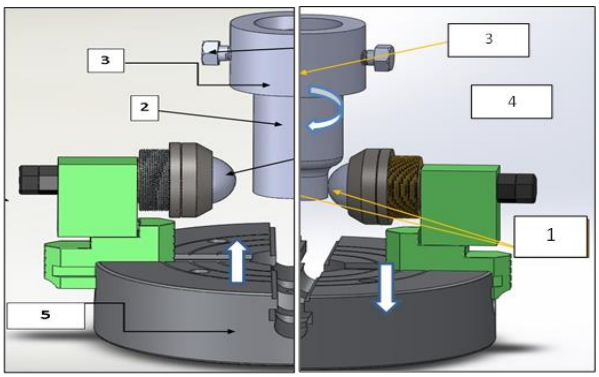

Fig. 1 the experimental setup of nosing process
A) Before forming process 1- Ballizing tool 2- Work piece (tube)
B) After forming process 3- Gripper. 4-lock bolts lathe chuck

The components of the load required for tube end forming in three coordinates are the axial, radial, and tangential components (Fx, Fy, and FZ), as shown in Fig. 2. The area in contact between sample and tool is formed due to tool penetration in the specimen. The interpretation of loads and projected area calculations and corrections during this analysis was done with the following assumptions:

(i) Spun material is isotropic, incompressible and alliterative.
(ii) Eliminate speed, spring back effects and temperature during the defacement.
(iii) During forming process, eliminate the hardening variation.
(iv) Uniform stress distribution along thickness (s_o).

The calculations of load components are done as follows:

$F_X = \bar{\sigma} A_X$ (1)
$F_Y = \bar{\sigma} A_Y$ (2)
$F_Z = \bar{\sigma} A_Z$ (3)

Where $\bar{\sigma}$ the average tensile stress, (F_T) is the resultant load, it expressed as showed:

$$F_T = \sqrt{F_X^2 + F_Y^2 + F_Z^2} \quad (4)$$

$$\bar{\sigma} = \frac{2}{\sqrt{3}} \bar{k} \sqrt{\left(\frac{1}{2} ln\left(\frac{s_f}{s_i}\right)\right)^2 + \left(ln\left(\frac{D}{d}\right)\right)^2} \quad (5)$$

Where (s_i) and (s_f)initial thickness of tube and final thickness of tube respectively, while (d) and (D) initial diameter of tube and final diameter of tube respectively. Instantaneously, contact surfaces appear between tube and tool during the process. Considering the process as quasi-stationary, this contact area maintains a constant. The intersection of the circumferential surface with the tool produced a sphere segment. It is difficult for some to describe such surfaces theoretically. However, the projected area confirmation is useful for further load component calculation. The sphere segment projected areas (Ax, Ay, and Az) are illustrated in Fig. 2 and calculated as shown:

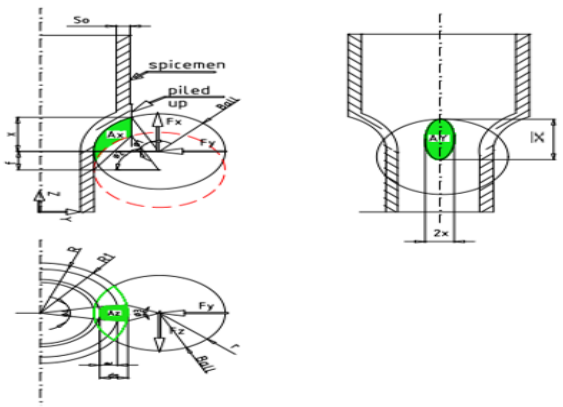

Fig. 2 Engineering drawing of projected area for ball impress in specimen

$$A_X = \frac{1}{2} r^2 \left(\frac{2\theta_1 - sin(2\theta_1)}{2}\right) + \left(\frac{1}{2}\left(f(ds + \overline{\Delta s})\right)\right) - r^2 \left(\frac{\theta_2 - sin(\theta_2)}{2}\right) \quad (6)$$

$$A_y = \left(\frac{\pi * X * \bar{X}}{2}\right) \quad (7)$$

$$A_Z = r^2\left(\frac{\theta_3 - \sin(\theta_3)}{2}\right) + R_1{}^2\left(\frac{\theta_4 - \sin(\theta_4)}{2}\right) \quad (8)$$

Where X, $\overline{X}$ are the distances, illustrated in Figure. (3) and calculated as follows:

$$X = \sqrt{r^2 - (R_1 - L)^2} \quad (9)$$

$$\overline{X} = \sqrt{R_1{}^2 - \left(\frac{R_1{}^2 + L^2 - r^2}{2L}\right)^2} \quad (10)$$

$$\theta_1 = \sin^{-1}\frac{X}{r} \quad (11)$$

$$\theta_2 = \sin^{-1}\frac{f}{r} \quad (12)$$

$$\theta_3 = \sin^{-1}\frac{\overline{X}}{r} \quad (13)$$

$$\theta_4 = 2\sin^{-1}\frac{X}{R_1} \quad (14)$$

Where R1 is outside radius of tube blank its defined byR_1=R+Δt, the distance between center of ball and center of specimen (L) defined by

$$L = R_1 + r \quad (15)$$

Where r is the radius of the forming ball.

By substituting equations 5 to 14 in equations 1, 2, and 3, the deformation loads components can be calculated as follows:

$$F_X = \left[\frac{2}{\sqrt{3}}\bar{k}\sqrt{\left(\frac{1}{2}\ln\left(\frac{s_f}{s_i}\right)\right)^2 + \left(\ln\left(\frac{D}{d}\right)\right)^2} * \begin{pmatrix} \frac{1}{2}r^2\left(\frac{(2\theta_1) - \sin(2\theta_1)}{2}\right) + \\ \left(\frac{1}{2}\left(f(ds + \overline{\Delta s})\right)\right) - \\ r^2\left(\frac{\theta_2 - \sin(\theta_2)}{2}\right) \end{pmatrix}\right] \quad (16)$$

$$F_Y = \left[\frac{2}{\sqrt{3}}\bar{k}\sqrt{\left(\frac{1}{2}\ln\left(\frac{s_f}{s_i}\right)\right)^2 + \left(\ln\left(\frac{D}{d}\right)\right)^2} \left(\left(\frac{\pi * \sqrt{r^2 - (R_1 - L)^2} * \left(\sqrt{R_1{}^2 - \left(\frac{R_1{}^2 + L^2 - r^2}{2L}\right)^2}\right)}{2}\right)\right)\right] \quad (17)$$

$$F_Z = \left[\frac{2}{\sqrt{3}}\bar{k}\sqrt{\left(\frac{1}{2}\ln\left(\frac{s_f}{s_i}\right)\right)^2 + \left(\ln\left(\frac{D}{d}\right)\right)^2} * \begin{pmatrix} r^2\left(\frac{\theta_3 - \sin(\theta_3)}{2}\right) \\ + \\ R_1{}^2\left(\frac{\theta_4 - \sin(\theta_4)}{2}\right) \end{pmatrix}\right] \quad (18)$$

Table (1) showed the required data for calculations, A comparison between calculated results due to mathematical model and experimental results was preamble and discussed in the following section.

Table (1) data used for mathematical calculations.

Parameter	*Value*
Strength coefficient (K), Mpa	79
Strain hardening exponent (n)	0.23
Initial wall thickness of tube (t), mm	3
workpiece outside radius before forming (R), mm	(38-50-60)
Axial feed rate (f), mm/min	0.3 - 1.21
Rotational speed (N), rpm	50 – 600

3 Material and Methods

3.1 Experimental Setup

Experimental setup as shown in Fig. 3 is consists of the Ballizing tools that are designed to work on a vertical milling machine and lathe machine, in which the work piece is held on one end by the gripper, which is unmovable in the axial direction, and the other end of the tube is free, which is formed by the balls to conduct the nosing process. The nosing tool is fixed to the end jaw of the lathe chuck and contacted when engaged with the work piece. The nosing tool is moved in the axial direction by the carriage of the milling machine, which is connected to the feed rate. The work piece free side is nosed, i.e., the tube free end diameter is reduced to the nosing value in one stroke. A cooling liquid is used during the process.

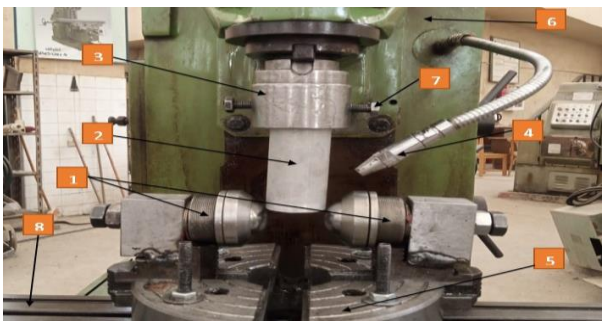

Fig.3 The Experimental setup of nosing process.

1- Ballizing tool. 2- Work piece (tube) 3- gripper. 4- lubricant nose. 5- lathe chuck. 6-mill head 7-lock bolts 8- Worktable

3.2 Tube ends forming tool

Fig. 4 showed the geometry of the nosing process using specific Ballizing forming tools that consist of a

large ball which sits upon a thrust bearing. The housing can contain a seal to clean the load ball as it rotates. The design greatly reduces friction and allows heavy loads.

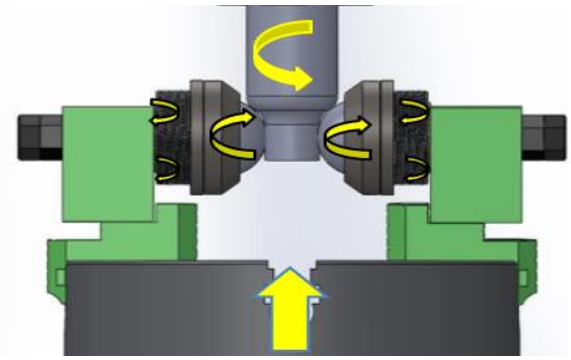

Fig.4 Nosing tool geometry

3.3 Used material

In this research, experiments done using aluminum tubes with outer diameter (d) 38,50,60 mm, wall-thickness (so) 3 mm and tube length (Lo) 150 mm. Aluminum as received tubes were used with n and K 0.13 and 117 MPa respectively. These samples were annealed after cutting in selected lengths by put it in furnace at 450 oC for 2 hours and let it in furnace until reach the room temperature. The samples values of n and K after annealing are 0.23 and 79 MPa respectively.

3.4 Measuring devices

In this process these devices used:
1) **Dynamometer device** connected with transducer linked with data logger sent output signals to computer after transforming it into volt, the computer converted it into charts and recordings.
2) **Dial gauge indicator** for sake of occurrences thickening and / or thinning, a measuring thickness was done along the nosed (deformed) section orthogonal to the wall thickness of tube.
3) **Vickers Hardness (HV)** device used to measure the hardness orthogonal to the circumference of the nosed part.
4) **Digital Vernier caliper** It was used to measure the roundness of nosing tube, the inner and outer diameter of the tube.

3.5 Working conditions:

Several experiments were carried out to conduct nosing specimens at different values of working conditions e.g. nosing ratio (NR = 3, 6, 9, and 12), rotational speed (N = 50, 92, 128, 240) rpm, Tube Diameter (38, 50, 60) mm and axial feed f (16, 29, 67,86) mm/min, these parameters are varied with each other.

3.6 Experimental Steps:

The Ballizing process begins by installing the tube sample in the milling machine using a gripper and installing the Ballizing tool on the milling machine carriage. The desired diameter reduction for the tube end is determined. The milling machine is turned on and the rotational speed and feeding rate are set, then the machine is set to automatic feed mode. Once complete, the tube is removed and inspected for defects. In summary, the process involves setting up the milling machine with the tube and tool, selecting the process parameters, performing the Ballizing operation with coolant, and then inspecting the finished product.

4 Results and Discussions

The results of an investigation into tube end forming using a Ballizing technique under different parameters. The key parameters studied are Feed rate, Speed, NR and Tube diameter. The effects of these parameters on the forming load required and the quality of the formed tube end are presented and discussed. The goal of the study is to understand how to optimize the Ballizing process for tube end forming by analyzing how the parameters affect the process outcomes.

4.1 Tube end formed by Ballizing tool.

The Fig. 5 a photographic image of successful samples of pipes that have been formed at their ends, it can be seen that the designed forming tool succeeded in shaping the pipe ends at different speeds and feeds for aluminum pipes of different diameters and different reduction ratios, using the Ballizing technique.

Fig.5 Successful samples

4.2 Effect of the selected parameters on forming load

In Fig. 6, the behavior of the nosing loads during the forming stroke, where the working conditions (N= 150 rpm and Feed = 0.24 mm/ rev) are taken, It is evident that the axial and radial components of the load increase rapidly compared to the tangential component, which appears to have a limited contribution. Initially, the axial load increases and remains higher than the radial component until after half of the forming stroke, this behavior can be attributed to the material flow occurring in the axial direction at the beginning of the forming process, which requires a higher force.

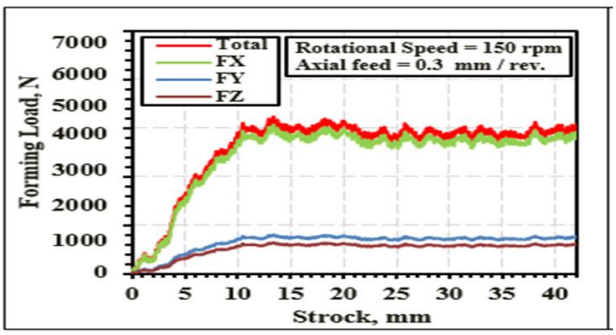

Fig. 6 Nosing load along the nosed section.

Subsequently, as the forming progresses, a higher load is necessary to complete the smoothing of the nosing. Understanding this behavior is important for optimizing process parameters to achieve the desired outcome.

4.3 Effects of NR on forming loads for different tube diameter

Fig. 7 represents the effect of nosing ratio (NR=(D/d)) on the forming load. It can be concluded from the Fig. that the forming load is increasing with any increase on NR. This may be due to the fact that the increasing in NR increases the contact area between forming tool and specimen which increases the load required for forming process.

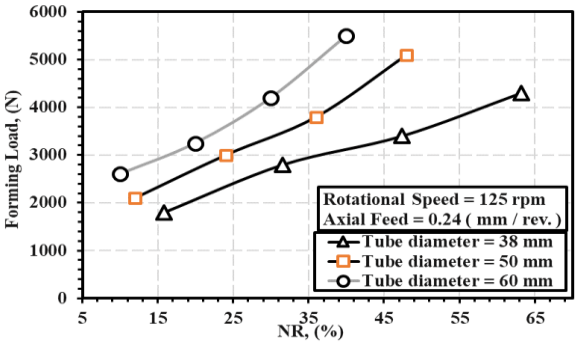

Fig.7 Forming load versus NR (%)

It can be seen from Fig. 8 that any increase in tube diameter increases the forming load. also, this is by reason of the growths of the contact area.

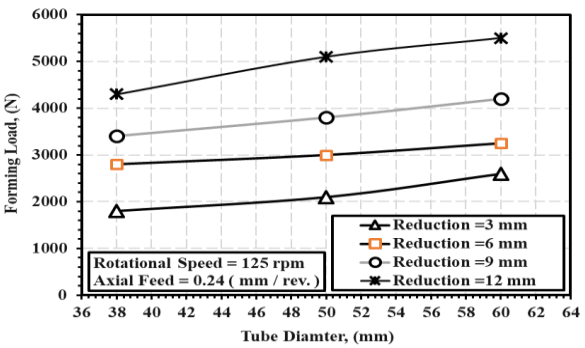

Fig. 8 Forming load versus Tube Diameter

Fig. 9 shows the relation between the achieved NR with the tube diameter, it can be concluded that the high NR can be achieved with small diameter any increase in tube diameters reduces the available NR, this is owing to the increases of the contact area increases the forming load which limits the NR.

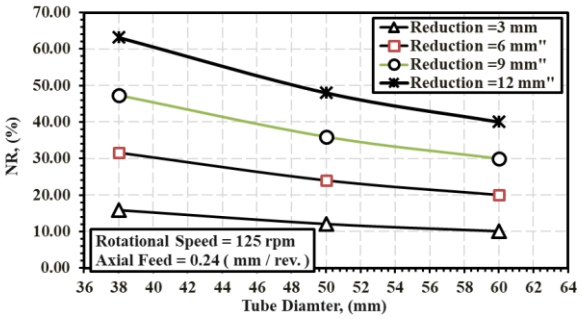

Fig. 9 NR (%) versus Tube Diameter

4.4 The effect of the process parameter on the thickness variation.

A measurement of the wall thickness perpendicular to the nosed (deformed) section of the tube was conducted using a digital dial gauge indicator. The nosed section, about 50 mm, was divided into positions along the nose as illustrated in Fig. 10. This Fig. provides an example of the thickness variation along the nosed section under working conditions such as f = 0.24 mm/rev, N = 125 rpm, and different tube diameter (mm). The results indicate that the thickness decreases at the start of the free side and gradually increases towards the other side, ultimately exceeding the original value along the deformed section. This thinning occurs because the circumference is strongly nosed at the beginning, while thickening occurs in the remaining portion of the deformed section due to the flow of material towards the radial side

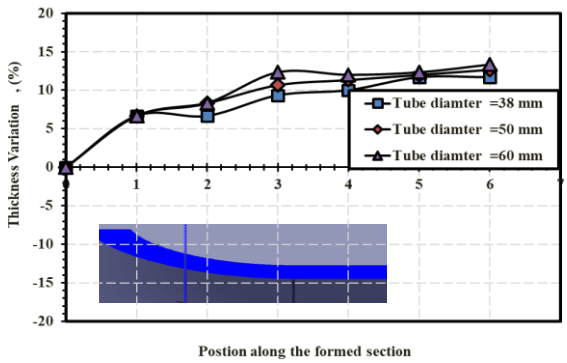

Fig. 10 Thickness variation at selected positions along nose section tube

4.5 The effect of the process parameter on the hardness.

During the nosing process, the contact of the work piece with the nosing tool results in surface hardening of the deformed part due to strain hardening. To investigate the effect of working conditions on the hardness of the nosed part, a micro hardness test was conducted.

A Vickers Hardness (Hv) device was used to measure the hardness perpendicularly on the circumference of the nosed part. Fig. 11 illustrates the trend of surface hardness variation along the nosed section, taking into account different reduction values, tube diameter, and working conditions such as N = 125 rpm and f = 0.24 mm/rev.

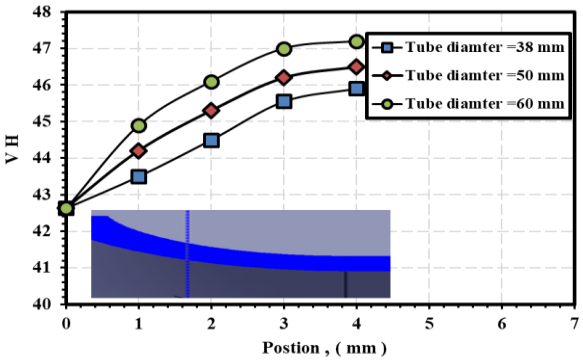

Fig. 11 The micro hardness along formed position (mm)

It is noteworthy that the measured hardness of all points is higher than the original value of 41 (N/mm2), indicating that work hardening occurs during the nosing process. Additionally, a slight decrease in the trend of surface hardness is observed from the free end to the chuck direction due to the decreasing of the contact area between the tool and work piece along the process stroke. Furthermore, an increase in spindle speed leads to an increase in the surface hardness of the nosed section. This is because higher rotational speeds result in more tool motions on the surface particles of the nosed section, leading to increased hardening.

4.6 Analytical and experimental comparison:

The comparison between the experimental and the analytical results are shown in Fig. 12. The results are the relation between the maximum load and the nosing ratio for a speed of 125 rpm and feed of 16, 29, 67 and 86 mm/min. It can be concluded that the error percentage is between 15 and 21%. This is may be due to that the effect of the strain hardening occurring during the forming process was not included in the theoretical analysis.

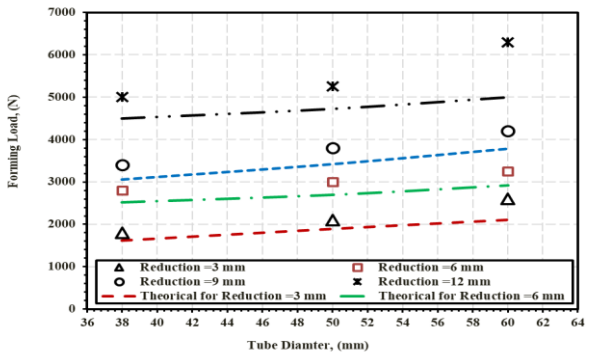

Fig. 12 Comparison between experimental and theoretical results.

5 Conclusion

Based on the experimental work, the following conclusions can be drawn:

1) The proposed tool succeeded in nosing the pipe ends of diameters (38-50-60) mm up to a nosing ratio of 63.16%, compared to 41% in past researches.

2) The proposed tool can be used with conventional lathe or milling machine which is very simple compared to other forming machines.

3) The quality of the products is significantly influenced by the investigated parameters, hardness of about 45 VH and a thickness variation of about 12%.

4) The comparison between the theoretical results and the experimental findings shows a close proximity of (79 - 85) %.

Acknowledgments

The authors would like to express their gratitude to faculty of engineering Minia university and the Industrial Education College at Beni-Suef University for their assistance and support.

References

[1] Ruch, R., P. Ludwig, and T. Maurer, Balancing Hydronic Systems in Multifamily Buildings. 2014, National Renewable Energy Lab.(NREL), Golden, CO (United States).

[2] Groover, M.P., Fundamentals of modern manufacturing: materials, processes, and systems. 2020: John Wiley & Sons.

[3] Ibrahim, Y.O., R.K. Abdel-Magied, and M.N. Elsheikh, An experimental investigation of tube-end nosing process using multi-functions spinning tool.

[4] Khalil Hazawi, A.R., R.K. Abdel-Magied, and M.N.J.T.I.J.o.A.M.T. Elsheikh, An experimental analysis of a flaring process for tube ends using a novel spinning tool. 2017. 92: p. 157-165.

[5] Oba, W., et al., Two-step forming for improvement of forming limit in rotary nosing with relieved die for fabrication of axisymmetric and eccentric nosed tubes. 2018. 262: p. 350-358.

[6] Wen, T., et al., Outwards and inwards crimping of tube ends by single-point incremental forming. 2017. 207: p. 854-859.

[7] Wilson, S., H. Long, and G.J.P.M. Garter, Non-axisymmetric tube spinning by offset rotation. 2018. 15: p. 1247-1254.

[8] Huang, C.-C., et al. The Influence of the Roller Forming Path on the Neck-Spinning Process of Tube at Elevated Temperature. in ASME International Mechanical Engineering Congress and Exposition. 2011.

[9] Jianguo, Y. and M.J.J.o.M.P.T. Makoto, An experimental study on paraxial spinning of one tube end. 2002. 128(1-3): p. 324-329.

[10] Jianguo, Y. and M.J.J.o.m.p.t. Makoto, An experimental study on spinning of taper shape on tube end. 2005. 166(3): p. 405-410.

[11] Huang, C.-C., et al., Finite element analysis on neck-spinning process of tube at elevated temperature. 2011. 56: p. 1039-1048.

[12] Kuboki, T., et al., Flexible rotary reduction of tube tips by dies with relief surfaces for attaining high forming limit and productivity. 2015. 64(1): p. 269-272.

[13] Mohamed, F.A., S.Z. El-Abden, and M.J.J.o.M.P.T. Abdel-Rahman, A rotary flange forming process on the lathe using a ball-shaped tool. 2005. 170(3): p. 501-508.

[14] Li, Y., et al., Comparison of radial forging between the two-and three-split dies of a thin-walled copper tube during tube sinking. 2014. 56: p. 822-832.

[15] Takahashi, Y., et al., Effects of neck length on occurrence of cracking in tube spinning. 2018. 15: p. 1200-1206.

[16] Zhao, C.-j., et al., Three-directional contact force model for the ball spinning of a thin-walled tube. 2019. 233(3): p. 500-507.

[17] Chunjiang, Z., et al., The analytical model of ball-spinning force for processing an annular groove on the inner wall of a steel tube. 2017. 91: p. 4183-4190.

[18] Kuss, M. and B.J.J.o.m.p.t. Buchmayr, Damage minimised ball spinning process design. 2016. 234: p. 10-17.

[19] Jiang, S., et al., Investigation of interface compatibility during ball spinning of composite tube of copper and aluminum. 2017. 88: p. 683-690.

[20] Akkus, N. and M.J.J.o.m.p.t. Kawahara, An experimental and analytical study on dome forming of seamless Al tube by spinning process. 2006. 173(2): p. 145-150.

[21] Xia, Q., et al., Finite element simulation and experimental investigation on the forming forces of 3D non-axisymmetrical tubes spinning. 2006. 48(7): p. 726-735.

[22] Xue, Z., et al. Effect of feed speed on aluminum alloy pipe neck-spinning process and deformation analysis via simulation. in MATEC Web of Conferences. 2016. EDP Sciences.

[23] Saied, E.K., et al., Combining conventional spinning with wall thickness reduction in one pass. 2019. 9(3): p. 1429-1436.

[24] Kwan, C.-T.J.J.o.M.P.T., An analysis of the eccentric nosing process of metal tubes. 2003. 140(1-3): p. 530-534.

[25] Kwan, C.-T., et al., An analysis of the nosing process of metal tubes. 2004. 23: p. 190-196.

[26] Manabe, K.-I. and H.J.J.o.m.w.t. Nishimura, Nosing of thin-walled tubes by circular curved dies. 1984. 10(3): p.

287-298.
[27] Gouveia, B., et al., Compression beading and nosing of thin-walled tubes using a die: experimental and theoretical investigation. 2006. 3: p. 7-16.
[28] Hua, F., et al., Three-dimensional finite element analysis of tube spinning. 2005. 168(1): p. 68-74.
[29] Murata, M., T. Kuboki, and T.J.J.o.m.p.t. Murai, Compression spinning of circular magnesium tube using heated roller tool. 2005. 162: p. 540-545.
[30] Jianguo, Y. and M.J.J.o.m.p.t. Makoto, Effects of indented feed of roller tool on parallel spinning of circular aluminum tube. 2002. 128(1-3): p. 274-279.
[31] Xia, Q., et al., Numerical simulation and experimental research on the multi-pass neck-spinning of non-axisymmetric offset tube. 2008. 206(1-3): p. 500-508.
[32] El-Abden, S.Z. And R.J.J.J.O.E.S. Atef, Finite element analysis and experimental investigations on hub forming in a sheet by the hole expanding technique. 2020. 48(1): p. 44-53.
[33] El-Abden, S.Z.J.J.O.A.E.T., Tube-to-sheet joints of dissimilar materials using combined plastic deformation process in single pass. 2021. 40(1): p. 109-128.
[34] Atia, K., et al., An investigation into a conventional spinning process combined with flow forming with simultaneously burnishing processes. 2021. 40(1): p. 97-107.
[35] Abdelhameed, R.A., et al., Study of aluminum tube cold nosing process into conical and hemispherical dies. 2022. 41(1): p. 113-124.